Available online at www.sciencedirect.com
ScienceDirect
Geochimica et Cosmochimica Acta xxx (2011) xxx–xxx
Geochimica et Cosmochimica Acta
www.elsevier.com/locate/gca

Dissolution of basalts and peridotite in seawater, in the presence of ligands, and CO_2: Implications for mineral sequestration of carbon dioxide

Domenik Wolff-Boenisch [a,*], Stefan Wenau [b], Sigurdur R. Gislason [a], Eric H. Oelkers [c]

[a] *Institute of Earth Sciences, University of Iceland, Sturlugata 7, 101 Reykjavik, Iceland*
[b] *MARUM – Centre for Marine Environmental Sciences, University of Bremen, Leobener Straße, 28359 Bremen, Germany*
[c] *GET, CNRS/UMR 5563, Université Paul Sabatier, 14 rue Edouard Belin, 31400 Toulouse, France*

Received 11 March 2011; accepted in revised form 6 July 2011

Abstract

Steady-state silica release rates (r_{Si}) from basaltic glass and crystalline basalt of similar chemical composition as well as dunitic peridotite have been determined in far-from-equilibrium dissolution experiments at 25 °C and pH 3.6 in (a) artificial seawater solutions under 4 bar pCO_2, (b) varying ionic strength solutions, including acidified natural seawater, (c) acidified natural seawater of varying fluoride concentrations, and (d) acidified natural seawater of varying dissolved organic carbon concentrations. Glassy and crystalline basalts exhibit similar r_{Si} in solutions of varying ionic strength and cation concentrations. Rates of all solids are found to increase by 0.3–0.5 log units in the presence of a pCO_2 of 4 bar compared to CO_2 pressure of the atmosphere. At atmospheric CO_2 pressure, basaltic glass dissolution rates were most increased by the addition of fluoride to solution whereas crystalline basalt rates were most enhanced by the addition of organic ligands. In contrast, peridotite does not display any significant ligand-promoting effect, either in the presence of fluoride or organic acids. Most significantly, Si release rates from the basalts are found to be not more than 0.6 log units slower than corresponding rates of the peridotite at all conditions considered in this study. This difference becomes negligible in seawater suggesting that for the purposes of in-situ mineral sequestration, CO_2-charged seawater injected into basalt might be nearly as efficient as injection into peridotite.

1. INTRODUCTION

The dissolution of mafic and ultramafic rocks in the presence of carbon dioxide is of great current interest due to the potential for carbon dioxide storage in basaltic and/or peridotitic rocks. This storage method involves converting gaseous/supercritical CO_2 into carbonate minerals for the safe and long-term storage of CO_2 (Seifritz, 1990; Lackner et al., 1995; Lackner, 2003; Metz et al., 2005; Oelkers and Schott, 2005). Consideration of the dissolution rates of various silicate minerals indicates that the most efficient source of the divalent cations essential for the carbonatization process are basalts and ultramafic rocks (e.g., Marini, 2006; McGrail et al., 2006; Matter et al., 2007; Kelemen and Matter, 2008; Oelkers et al., 2008a; Andreani et al., 2009; Prigiobbe et al., 2009b; Schaef and McGrail, 2009; Shikazono et al., 2009; Schaef et al., 2010; Gislason et al., 2010). To limit the risk associated with buoyancy and to facilitate host rock/CO_2 reactions, it is advantageous to dissolve this gas into an aqueous solution prior to its injection into the subsurface. CO_2 dissolution, however, requires large water volumes (Gislason et al., 2010) that may not be available due to insufficient groundwater sources, low recharge rates, or inefficient water management (cf. Oelkers et al., 2011; Schwartz and Ibaraki, 2011). In such cases, mineral sequestration may only

* Corresponding author.
E-mail address: boenisch@raunvis.hi.is (D. Wolff-Boenisch).

0016-7037/$ - see front matter © 2011 Elsevier Ltd. All rights reserved.
doi:10.1016/j.gca.2011.07.004

become a viable option for carbon storage when seawater is used for the dissolution of CO_2 before injection. Towards the better understanding of the potential applicability of seawater during carbon mineralization efforts, the dissolution rates of basalt and peridotite have been determined in CO_2-rich reactive fluids, including natural and artificial seawater. The purpose of this study is to report the results of these measurements and to use them to assess the potential of seawater to be used for carbonation purposes preceding mineral sequestration.

The interaction of seawater with mafic and ultramafic rocks is significant to a number of natural processes. For example, hydrothermal alteration of mid-ocean ridge basalts plays a large role in the global cycling of the elements (e.g., Bischoff and Dickson, 1975; Seyfried and Bischoff, 1977, 1979, 1981; Mottl and Holland, 1978; Seyfried and Mottl, 1982; Humphris et al., 1995; German et al., 2004; Lowell et al., 2008). The interaction of low temperature, acidic, CO_2-rich seawater such as investigated in this study can also lead to extensive carbonatization in natural systems (Robins and Tysseland, 1983; Greenough and Papezik, 1985; Veizer et al., 1989; Nakamura and Kato, 2004; Rogers et al., 2006).

2. MATERIALS AND METHODS

2.1. Rocks

The basaltic glass and crystalline basalt used in this study, referred to as 'G' and 'X' in some figures and tables, were collected from the Stapafell Mountain in SW Iceland. The dissolution behaviour of these basalts has been previously studied (Oelkers and Gislason, 2001; Gislason and Oelkers, 2003; Flaathen et al., 2010; Stockmann et al., 2011; Gudbrandsson et al., 2011). Their chemical compositions, normalized to one Si, are listed in Table 1a. The elemental composition of the basaltic glass is nearly identical to that of the crystalline basalt. In contrast to the glass, the crystalline basalt is a heterogeneous multi-phase solid consisting of 41 vol% labradoritic plagioclase, 34 vol% augitic clinopyroxene, 16 vol% forsteritic olivine, and minor iron oxides and interstitial glass. The mineralogical composition of this rock is summarized in Table 1b. Further details of these rocks, including their chemical composition as determined by X-ray fluorescence spectroscopy as well as scanning electron microscope images of their surfaces can be found in Stockmann et al. (2011) and Gudbrandsson et al. (2011), respectively.

The peridotite (referred to as 'P' in some figures and tables) is the 'green' variety from the Gusdal locality in the Almklovdalen peridotite complex within the Western Gneiss Region, southern Norway. Details on its genesis and petrology can be found in Kostenko et al. (2002). Mineralogically, the peridotite is a chlorite dunite consisting of 90–95 vol% olivine and minor Mg–clinochlore. Cr–spinel was not detected by X-ray diffraction and has therefore not been listed as a phase in Table 1b. However, electron microprobe analysis confirmed its presence through a characteristic Cr peak.

All solids were dried at room temperature for several days before being ground with a jaw crusher. The material was dry sieved to obtain the 45–125 μm size fraction. This size fraction was gravitationally settled to remove fine particles, then cleaned ultrasonically five times in deionized water and then in acetone. The resulting powder was oven-dried at 50 °C for several days. The BET specific surface area of the cleaned powders was determined via 3-point krypton adsorption using a Quantachrome Gas Sorption system. Resulting BET surface areas are listed in Table 1a, together with corresponding specific geometric surface areas (A_{geo}) that were determined by dividing the number 6 (= number of faces of a perfect cube) by the product of particle density and average particle diameter.

2.2. Reactive fluids

The natural seawater used in some experiments had a normal salinity of 35.1‰ and was collected in acid washed 27 L polypropylene buckets at 988 m depth off the southwest shore of Iceland (64°20′N; 27°57′W). This seawater was pumped through a Barnstead® activated charcoal pre-treatment cartridge followed inline by a 0.15 μm ColeParmer® carbon-block membrane cartridge to remove organics, bacteria, and suspended material. It was subsequently stored at 4 °C in the dark and warmed up to room temperature overnight prior to its use.

In addition to the experiments run in natural seawater, further experiments were performed in artificial seawater and other aqueous solutions. These solutions were created by dissolving Merck™ or Sigma–Aldrich™ chemicals in deionized Millipore™ water. All chemicals used were reagent grade other than the siderophore desferrioxamine B (DFOB) which was ⩾92.5% pure. Artificial seawater was created to contain the solute concentrations for the ions Na, K, Mg, Ca, chloride, sulphate, (bi)carbonate, and fluoride equal to that proposed by Millero (2003). DFOB was

Table 1a
Chemical composition and surface areas of the basaltic glass (G), crystalline basalt (X), and peridotite (P) used in this study normalized to one silicon. The composition of two other basaltic glasses considered in this study (SS, HEI) whose composition was previously reported (Wolff-Boenisch et al., 2004b) are also provided.

Rock	Chemical composition	A_{BET} (cm^2/g)	A_{geo} (cm^2/g)
G	$Si_{1.000}\ Al_{0.365}\ Mg_{0.294}\ Ca_{0.263}\ Na_{0.081}\ K_{0.008}\ Ti_{0.025}\ P_{0.004}\ Mn_{0.003}\ Fe_{0.191}\ O_{3.403}$	5878	251
X	$Si_{1.000}\ Al_{0.329}\ Mg_{0.310}\ Ca_{0.273}\ Na_{0.061}\ K_{0.007}\ Ti_{0.025}\ P_{0.003}\ Mn_{0.003}\ Fe(II)_{0.174}\ Fe(III)_{0.019}\ O_{3.374}$	7030	255
P	$Si_{1.000}\ Al_{0.017}\ Mg_{1.639}\ Fe(II)_{0.120}\ Cr_{0.005}\ Mn_{0.002}\ O_{3.795}$	3286	232
SS	$Si_{1.000}\ Al_{0.414}\ Mg_{0.189}\ Ca_{0.228}\ Na_{0.150}\ K_{0.018}\ Ti_{0.039}\ P_{0.006}\ Mn_{0.003}\ Fe(II)_{0.174}\ Fe(III)_{0.042}\ O_{3.457}$	1945	255
HEI	$Si_{1.000}\ Al_{0.377}\ Mg_{0.075}\ Ca_{0.147}\ Na_{0.224}\ K_{0.040}\ Ti_{0.033}\ P_{0.013}\ Mn_{0.004}\ Fe(II)_{0.129}\ Fe(III)_{0.056}\ O_{3.238}$	710	272

Please cite this article in press as: Wolff-Boenisch D., et al. Dissolution of basalts and peridotite in seawater, in the presence of ligands, and CO_2: Implications for mineral sequestration of carbon dioxide. *Geochim. Cosmochim. Acta* (2011), doi:10.1016/j.gca.2011.07.004

Table 1b
Mineralogical composition in volume percent of the basalts and peridotite.

Rock	Mineralogical composition
G, SS, HEI	100% glass
X	41% labradorite (An_{65}), 34% augite, 16% olivine (Fo_{85}), 5% iron oxides, 4% glass
P	90–95% olivine (Fo_{92}), ~5% Mg–clinochlore (Mg/(Mg + Fe) = 95–97 mol%)

used in this study as a proxy for siderophores present in seawater. Marine siderophores are known to be major iron chelators (Macrellis et al., 2001; Yoshida et al., 2002) which may serve a pivotal role in the supply of dissolved iron in many parts of the oceans.

The Si, Ti, Na, K, Mg, Ca, Fe, Al, and Mn concentrations of all inlet and outlet fluids were measured by inductively coupled argon plasma using a Spectro Vision optical emission spectrometer. Fluoride was determined using a Cole-Parmer® fluoride specific electrode and DOC was assessed via high temperature catalytic oxidation with non-dispersive infrared detection at the Umea Marine Sciences Centre, Sweden.

2.3. Experimental design

In total four distinct experimental series were performed on the three rocks. Each series was designed to determine the effects of specific fluid components on the dissolution kinetics of these solids. Series SWC focussed on the effect of the chemical components of seawater on dissolution rates, series I focussed on the effect of varying ionic strength, and series F and DOC focussed on the effects of changing fluoride and dissolved organic carbon concentrations, respectively. Table 2 provides further details about these four different experimental series.

Two different experimental designs were used in this study. Series SWC was performed in the presence of 4 bar pCO_2, while the pCO_2 of the other three experimental series (I, F, DOC) was fixed by atmospheric equilibrium. The continuously elevated pCO_2 in series SWC leads to a measured reactive fluid pH of 3.6 due to carbonic acid dissociation. To allow direct comparison with the results of this series, HCl was added to the inlet fluids of the other three experimental series to obtain a comparable pH. A schematic illustration of the pressurized reactor system used for series SWC is shown in Fig. 1. This reactor system allows the continuous control and maintenance of constant elevated CO_2 pressure over the entire duration of the experimental series. A high pressure liquid chromatography pump delivered the inlet fluid into the Parr Instrument™ reactor at rates from 1 to 2 ml/min. The reactor temperature was maintained at 25 °C with a heating sleeve. The inlet solution was mixed with CO_2 from a 200 L gas cylinder at the reactor inlet. This fluid/CO_2 mixture was injected into the bottom of the reactor via a dip tube to ensure maximum contact time of liquid and gas. The 300 ml reactor was loaded with 4–5 g of powdered rock prior to the start of each experiment. The fluid/solid suspension was stirred constantly by a magnetic stirrer at approximately 300 rpm. To obtain maximum gas dispersion into the liquid, the stirrer was fitted with a special gas entrainment impeller with gas dispersion ports located at its tips. The CO_2 was thus continuously re-circulated from the head space above into the liquid through the impeller. The pressurized outlet fluid passed through a custom-made Teflon® pH cell containing high P/T pH electrodes (Corr Instruments, Texas) connected to a pH meter. From the pH electrode chamber, the fluid passed through a titanium back pressure regulator whose pressure was regulated with nitrogen. Samples passed through a 2 μm titanium filter when exiting the reactor and were further filtered at the outlet through a 0.2 μm cellulose acetate filter and acidified with 0.5% concentrated suprapure HNO_3. All wet components of the system were either made of Teflon®, PEEK (polyetheretherketone) or titanium since any steel alloy could corrode at the ionic strength and pH of the reactive fluids.

The reactor was operated for 48 h before the first sample was taken. Sample collection was timed to allow 2–3 residence times to pass between each sampling. The residence time is defined as the reactor volume divided by the fluid flow rate and ranged from 3 to 5 h, depending on the experiment. Steady-state was assumed when four consecutive rate determinations from Si outlet concentrations showed a standard deviation of $\leqslant$0.15 log units. This usually occurred within 3–4 days. Steady-state Si release rates were obtained for each inlet fluid composition.

At the onset of the experimental series SWC, the inlet fluid consisted of a Na, K, Mg, Ca chloride solution with composition mimicking seawater. After reaching steady-state, 68 μmolal of NaF was added to the original chloride inlet fluid. On attainment of a second steady-state, 28 mmolal of $MgSO_4$ was added and a new steady-state reached. This was followed by the addition of 10 μmolal of DFOB to this inlet fluid and achievement of a further steady state. Finally, 1.75 mmolal $NaHCO_3$ and 0.27 mmolal Na_2CO_3 were added together to this inlet fluid. This final inlet fluid had a composition and ionic strength nearly identical to that of typical seawater (Millero, 2003).

Experimental series I was performed in a similar manner as series SWC in that an inlet fluid was pumped through a reactor filled with powdered rock, this time, however, without added CO_2 pressure. As such, no gas cylinder, back pressure regulator or pH cell was required. The reactor system used for these experiments is illustrated in Fig. 2 and consisted of three Parr Instruments™ titanium reactors connected by a mixing tee joint with the incoming fluid. In this way the dissolution kinetics of three different materials can be simultaneously measured at same conditions. At the start of this experimental series each reactor was filled with 4–5 g of solid rock material. All reactor components in contact with the fluid phase were either made of Teflon®, PEEK, titanium, or Hastelloy® 276 to avoid corrosion.

As was the case in experimental series SWC, experimental series I consisted of a set of sequential steady-state conditions for inlet fluids of distinct compositions (cf. Table 2). Beginning with a 10 mmol/kg NH_4Cl inlet fluid, subsequent

Please cite this article in press as: Wolff-Boenisch D., et al. Dissolution of basalts and peridotite in seawater, in the presence of ligands, and CO_2: Implications for mineral sequestration of carbon dioxide. *Geochim. Cosmochim. Acta* (2011), doi:10.1016/j.gca.2011.07.004

Table 2
Chemical composition of all inlet solutions used and Si release rates obtained in the present study. The prefixes on the reference codes correspond to the experimental series SWC, I, F, and DOC which explore the effect on rates of seawater components, ionic strength, fluoride, and dissolved organic carbon, respectively. The abbreviations G, X, and P designate basaltic glass, crystalline basalt, and peridotite.

Reference code	Inlet solution composition[a]	Ionic strength[b] (mol/kg)	Exp. duration (h)	pCO_2 (bar)	pH in	pH out[c]	Log $r_{Si,geo}$[d]		
							G	X	P
SWC-Cl	469 mm NaCl, 10 mm KCl 53 mm $MgCl_2$, 10 mm $CaCl_2$	0.697	102	4	3.53	3.76	−8.42	−8.14	−7.65
SWC-F	68 μm NaF added	0.697	174	4	3.53	3.88	−7.95	−7.99	−7.55
SWC-SO_4	28 mm $MgSO_4$ added	0.691	270	4	3.59	3.94	−7.93	−7.98	−7.54
SWC-DFOB	10 μm DFOB added	0.691	342	4	3.59	3.94	−7.96	−8.03	−7.52
SWC-CO_3	1.75 mm $NaHCO_3$ and 0.27 mm Na_2CO_3 added[e]	0.690	438	4	4.31	4.64	−8.12	−8.29	−7.70
I-NH_4	10 mm NH_4Cl, HCl	0.010	96	at[f]	3.60	3.77	−8.85	−8.61	−8.04
I-K	22 mm KCl, HCl	0.023	169	at	3.47	3.54	−8.79	−8.50	−7.95
I-Ca	10 mm $CaCl_2$, HCl	0.031	265	at	3.63	3.91	−8.54	−8.64	−8.03
I-Mg	53 mm $MgCl_2$, HCl	0.160	337	at	3.56	4.20	−8.35	−8.23	−8.00
I-Na	482 mm NaCl, HCl	0.483	433	at	3.51	3.99	−8.49	−8.38	−8.10
I-SW*	SW[g], HCl	0.664	601	at	3.68	4.73	−8.26	−8.35	−8.05
F-67	SW, HCl, 67 μm NaF	0.668	169	at	3.57	5.14	−8.14	−8.32	−7.90
F-120	SW, HCl, 112 μm NaF	0.668	242	at	3.60	5.27	−8.16	−8.20	−7.96
F-180	SW, HCl, 166 μm NaF	0.668	338	at	3.63	5.64	−8.05	−8.15	−7.92
F-240	SW, HCl, 235 μm NaF	0.668	409	at	3.71	5.66	−7.96	−8.00	−7.75
DOC-SW	SW, HCl	0.668	73	at	3.62	5.82	−8.30	−8.46	−8.13
DOC-DFOB	SW, HCl, 120 μm DFOB	0.668	170	at	3.64	5.51	−8.11	−7.99	−8.05
DOC-Ox	SW, HCl, 120 μm oxalic acid	0.668	241	at	3.56	5.79	−8.27	−7.95	−7.98
DOC-Cit	SW, HCl, 120 μm citric acid	0.668	336	at	3.63	5.77	−8.30	−8.08	−8.10

[a] All *molal* concentrations were calculated based on the mass of chemical added, only fluoride in the 'F' series was analyzed.
[b] Determined with PHREEQC.
[c] Corresponds to the pH measured in the in-line cell for the 'SWC' experiments.
[d] Rates are in units of (mol/m^2/s).
[e] Corresponds to a bicarbonate alkalinity of 2.29 mequiv.
[f] Atmospheric.
[g] Natural seawater.

steady-states were obtained by *replacing* the inlet fluid, first with a KCl solution, then a $CaCl_2$ solution, then a $MgCl_2$ solution, and finally a NaCl solution. The pH of all these inlet fluids was adjusted to pH 3.6 with HCl to imitate the pH of the SWC series and the concentration of each of these chloride inlet solutions was selected to correspond to that of seawater for the given cation. After attainment of steady-state with the NaCl inlet fluid, this fluid was replaced with natural seawater plus sufficient HCl to lower its pH to 3.6.

Two additional experimental series, F and DOC, were performed. These sets were run in the same reactors as used for series I described above. Likewise, a series of distinct steady-state dissolution rate measurements were obtained in conditions of chemically varying fluids. The initial inlet fluid for experimental series F was a natural seawater solution adjusted to pH 3.6 by adding HCl. This natural seawater already contains 67 μmolal fluoride, in close agreement to the literature for typical seawater (Millero, 2003). After reaching steady-state, NaF was added *sequentially* to this inlet fluid to create inlet fluids containing fluoride concentrations of 120, 180, and 240 μmolal, respectively. Similarly, the initial inlet fluid for experimental series DOC was also natural seawater adjusted to pH 3.6 with HCl. Subsequent reactive inlet fluids were composed of (1) this acidified seawater plus 120 μmolal DFOB, (2) this acidified seawater plus 120 μmolal oxalic acid, and (3) this acidified seawater plus 120 μmolal of citric acid (cf. Table 2).

3. THEORETICAL BACKGROUND

The standard state adopted in this study is that of unit activity of pure minerals and H_2O at any temperature and pressure. For aqueous species other than H_2O, the standard state is unit activity of species in a hypothetical one molal solution referenced to infinite dilution at any temperature and pressure. All thermodynamic calculations reported in this study were performed using the geochemical modelling code PHREEQC (Parkhurst and Appelo, 1999) together with its phreeqc.dat database.

Rates determined in the present study are based on Si release. This choice was made for several reasons. First, Si is generally the element holding together the mineral or glass structure; its release requires the dissolution of most minerals (cf. Oelkers, 2001b). Secondly, other solute choices, like Mg, Ca, Fe, or Al, are either present in very small quantities (e.g., Al and Ca in peridotite) or released preferentially (e.g., Mg and Fe in crystalline basalt). Furthermore, many experiments in this study were carried out in artificial and

Please cite this article in press as: Wolff-Boenisch D., et al. Dissolution of basalts and peridotite in seawater, in the presence of ligands, and CO_2: Implications for mineral sequestration of carbon dioxide. *Geochim. Cosmochim. Acta* (2011), doi:10.1016/j.gca.2011.07.004

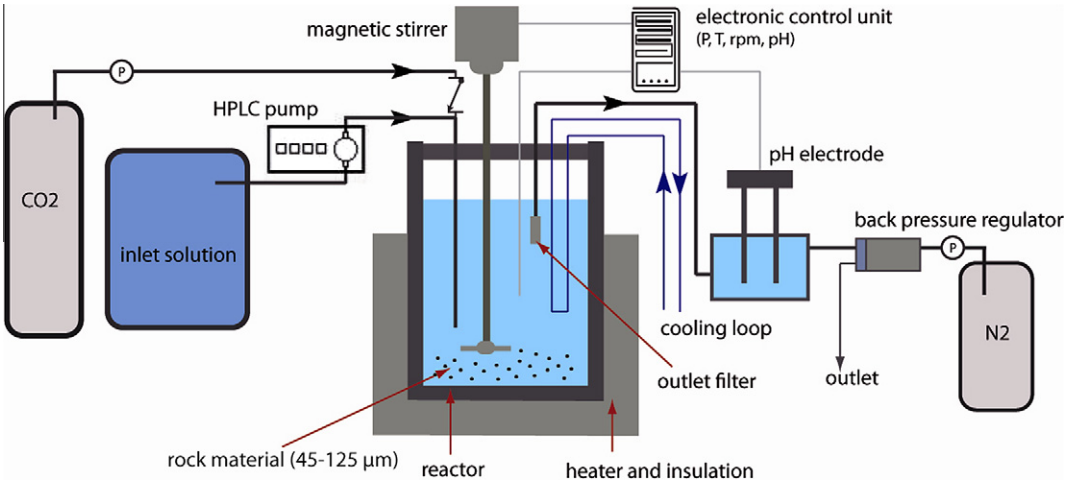

Fig. 1. Experimental set-up used for experimental series SWC in the presence of 4 bar CO_2 pressure. The inlet fluid was delivered to the titanium mixed-flow reactor via a high pressure liquid chromatography (HPLC) pump while, simultaneously, gaseous CO_2 entered the same dip tube through a hose and a check valve. The outlet fluid was pumped across an inline pressurized pH cell and exited through a titanium back pressure regulator whose pressure was controlled with nitrogen.

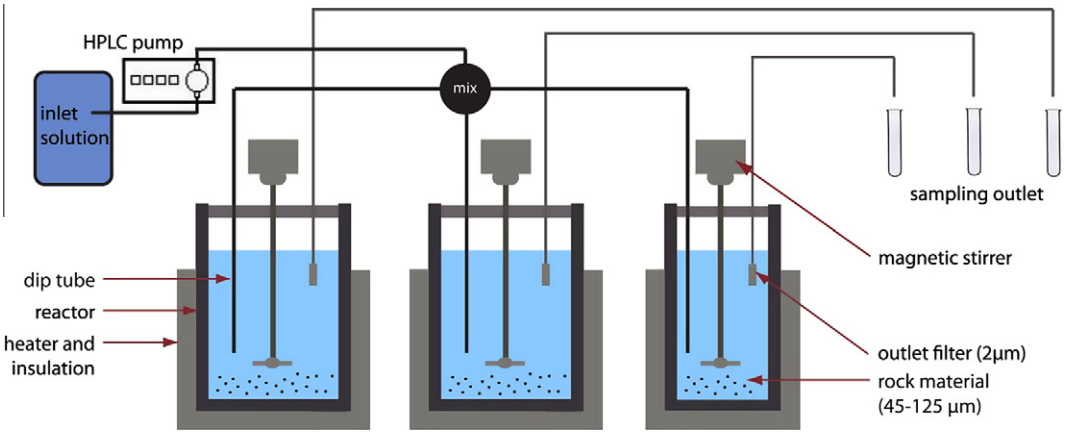

Fig. 2. Experimental set-up used for experimental series I, F, and DOC. The inlet fluid was delivered to the three titanium mixed-flow reactors via a high pressure liquid chromatography (HPLC) pump and a mixing tee ('mix') joint. The 300 ml reactors on the left held basaltic glass and crystalline basalt, respectively while the 100 ml reactor to the right hosted peridotite.

natural seawater rendering it impossible to quantify the minute difference between inlet and outlet Ca and Mg concentrations required for rate determinations. Si release rates ($r_{Si,geo}$) were generated using:

$$r_{Si,geo} = F \cdot C_{Si}/(A_{geo} \cdot m) \quad (1)$$

where F is the pump flowrate, C_{Si} stands for the concentration of Si in the outlet fluid, A_{geo} denotes the specific geometric surface area (cf. Table 1a), and m represents the initial mass of material in the reactor. Rates in this study were normalized to geometric specific surface area, which for the case of glass dissolution was found to be more consistent than normalizing rates to the BET specific surface area (Wolff-Boenisch et al., 2004b).

The dissolution of glassy basalt can be treated as a homogeneous one-phase system consisting 100% of basaltic glass. Back scattering images from a scanning electron microscope confirm that while microcrystalline phases are present, they are confined within the glass shards (Wolff-Boenisch, 2004). Consistent with the dissolution mechanisms of many aluminosilicate minerals (Oelkers et al., 1994, 2008b; Schott and Oelkers, 1995; Devidal et al., 1997; Oelkers and Schott, 1999; Harouiya and Oelkers, 2004; Lowson et al., 2005), including plagioclases (Oelkers and Schott, 1998), the rate controlling step in the dissolution of basaltic glass is the breaking of partially liberated Si–O tetrahedra formed by Al for proton exchange reactions (Oelkers and Gislason, 2001; Gislason and Oelkers, 2003; Wolff-Boenisch et al., 2004a; Stockmann et al., 2011). In accord with this mechanism, basaltic glass forward dissolution rates (r_{glass}) can be described using (Oelkers and Gislason, 2001):

$$r_{glass} = k(a^3_{H^+}/a_{Al^{3+}})^n \quad (2)$$

Please cite this article in press as: Wolff-Boenisch D., et al. Dissolution of basalts and peridotite in seawater, in the presence of ligands, and CO_2: Implications for mineral sequestration of carbon dioxide. *Geochim. Cosmochim. Acta* (2011), doi:10.1016/j.gca.2011.07.004

where k stands for a rate constant, n represents the reaction order equal to 1/3 and a_i corresponds to the activity of the subscripted aqueous species. The form of Eq. (2) is due to the stoichiometry of the proton for Al exchange reaction, which balances charge, and the reaction order n corresponds to the number of partially liberated Si atoms created by each exchange reaction. In accord with Eq. (2), any ligand that affects the aqueous speciation of Al will affect basaltic glass dissolution rates.

The peridotite consists mainly of forsteritic olivine plus minor amounts of Mg–clinochlore and traces of Cr–spinel. Because of the much lower dissolution rate of chlorite compared to forsterite at acidic conditions (Brandt et al., 2003; Lowson et al., 2005), the dissolution behaviour of this peridotite should be similar to that of pure olivine. A large number of studies have provided forsterite dissolution rates (e.g., Kuo and Kirkpatrick, 1985; Wogelius and Walther, 1991, 1992; Chen and Brantley, 2000; de Leeuw et al., 2000; Pokrovsky and Schott, 2000; Rosso and Rimstidt, 2000; Oelkers, 2001a; Hänchen et al., 2006; Morris and Wogelius, 2008; Olsen and Rimstidt, 2008; Prigiobbe et al., 2009a,b). An equation describing far-from-equilibrium forsterite dissolution (r_{Fo}) under acidic conditions, based on the assumption that the breaking of the silica-rich/magnesium-deficient $\{>Si_2O–H^+\}$ surface complex controls dissolution rates, is given by (Pokrovsky and Schott, 2000):

$$r_{Fo} = k\{> Si_2O–H^+\} \quad (3)$$

where k represents a rate constant and $\{>Si_2O–H^+\}$ stands for the $>Si_2O–H^+$ surface species concentration. The $\{>Si_2O–H^+\}$ complex is formed by exchange of two protons for a Mg atom on the forsterite surface followed by polymerization of partially protonated SiO_4 tetrahedra and rate-controlling proton penetration into the leached layer and its adsorption on silica dimers. According to this rate expression pH is the most crucial factor influencing forsterite dissolution.

Crystalline basalt is comprised of three major mineral phases, augite, labradorite, and forsterite. Its dissolution behaviour over the entire pH range was found to correspond approximately to the sum of the dissolution rates of each constituent normalized to its volume fraction in accord with (Gudbrandsson et al., 2011):

$$r_{i,j} = \sum_{k=0}^{N} \frac{A_{j,k}}{A_j} v_{i,k} r_{j,k} = \frac{A_{j,plag}}{A_j} v_{i,plag} r_{j,plag} + \frac{A_{j,ol}}{A_j} v_{i,ol} r_{j,ol} + \frac{A_{j,py}}{A_j} v_{i,py} r_{j,py} \quad (4)$$

where $r_{j,k}$ refers to the dissolution rate of the kth mineral (plagioclase, olivine, pyroxene) normalized to the jth surface area, $v_{i,k}$ designates the stoichiometric number of the ith element in the kth mineral, $A_{j,k}$ symbolizes the jth specific surface area of the kth mineral and A_j is the overall surface area.

Plagioclase forward dissolution rates can be described using the same equation as Eq. (2) (Oelkers and Schott, 1998). Most pyroxene dissolution studies have focussed principally on diopside (Knauss et al., 1993; Chen and Brantley, 2000; Golubev et al., 2005; Dixit and Carroll, 2007; Daval et al., 2010) and much less so on augite (Siegel and Pfannkuch, 1984). Pyroxene forward dissolution rates decrease continuously with increasing pH and are mildly inhibited by increasing divalent metal cation concentration. Assuming forward pyroxene dissolution rates (r_{py}) are controlled by the breaking of partially liberated Si–O tetrahedra formed by divalent metal for proton exchange reactions they can be described in accord with (Oelkers and Schott, 2001):

$$r_{py} = k(a^2_{H^+}/a_{M^{2+}})^n \quad (5)$$

where again k designates a rate constant, n stands for a reaction order equal to 1/8, and M represents the major divalent metal of the pyroxene. Eqs. (2)–(5) suffice to describe the dissolution behaviour of all major phases constituting the rocks dissolved in this study. They will be used below to describe measured Si release rates as a function of fluid chemistry.

4. RESULTS AND DISCUSSION

4.1. Experimental series SWC

Experimental series SWC was aimed at assessing the effect of various seawater components at near constant ionic strength on rock dissolution rates at elevated CO_2 partial pressure. Fig. 3 is an example of the variation in steady-state Si release rates over time encountered in the experiments. This figure illustrates results from the basaltic glass dissolution experiments. Individual rates were determined at sampling intervals of approximately three residence times and averaged to yield the r_{Si} values shown in Fig. 4 and listed in Table 2 for the three rock types. Crystalline and glassy basalt dissolution kinetics exhibit similar Si release rates whereas Si is released 0.4–0.6 log units faster from peridotite. Given the dunitic character of the peridotite, this observation is close to the average 0.7 log unit difference found between forsterite and basaltic glass dissolution rates at pH 4 reported by Wolff-Boenisch et al. (2006). The addition of 68 μmolal NaF to the initial high ionic strength reactive fluid increases the glass rate threefold. This dissolution promoting effect of fluoride has been well established for silicate minerals (e.g., Grandstaff, 1986; Steel et al., 2001; Harouiya and Oelkers, 2004) and volcanic glasses (Wolff-Boenisch et al., 2004a). In the latter case, the dissolution promoting effect was explained by the interaction of fluoride with aluminium released from the glasses reducing thus the aqueous activity of Al^{3+} in the fluid (see Eq. (2)). In contrast, the Si release rates from crystalline basalt and peridotite are only slightly increased by the addition of F to the reactive fluid. The relatively small effect of F on r_{Si} of these rocks stems from the fact that their dissolution is dominated by olivine and/or clinopyroxene at the low pH of these experiments (cf. Gudbrandsson et al., 2011). Consistent with Eqs. (3) and (4), olivine and clinopyroxene dissolution rates are relatively insensitive to aqueous fluoride concentration. The Si release rates then remain close to constant for all rocks, irrespective of the further, *sequential* addition of 28 mmolal $MgSO_4$ and 10 μmolal DFOB. This

Please cite this article in press as: Wolff-Boenisch D., et al. Dissolution of basalts and peridotite in seawater, in the presence of ligands, and CO_2: Implications for mineral sequestration of carbon dioxide. *Geochim. Cosmochim. Acta* (2011), doi:10.1016/j.gca.2011.07.004

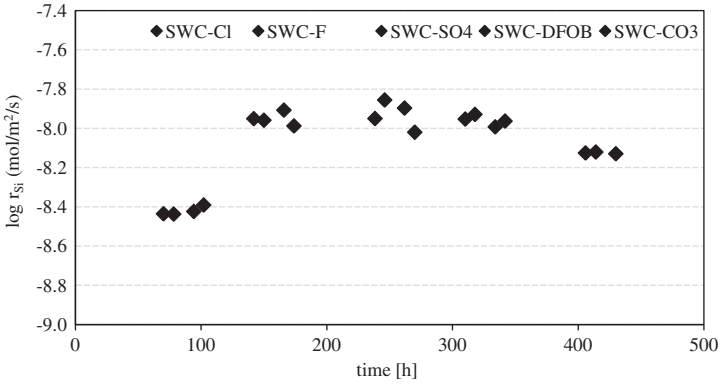

Fig. 3. Steady-state silica release rates as a function of time during the dissolution of the basaltic glass during experimental series SWC. This series consisted of a set of dissolution experiments performed first in a solution containing the same NaCl, KCl, $CaCl_2$, and $MgCl_2$ concentration as seawater. The ligands F, SO_4, DFOB, and CO_3 were added *sequentially* to this reactive fluid to determine the effect of each seawater component on rates. Steady-state was assumed when at least three consecutive samples yielded comparable Si release rates. Sampling intervals corresponded to approximately three residence times.

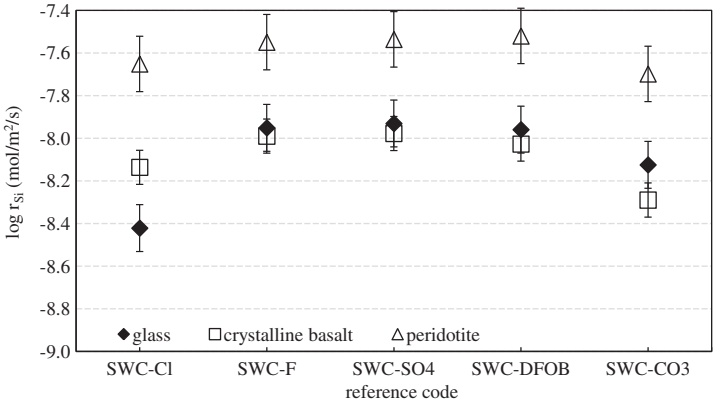

Fig. 4. Variation in steady-state Si release rates of the basaltic glass, crystalline basalt, and peridotite as a function of fluid chemistry in the SWC series. The ionic strength was near constant at 690–697 mmol/kg in all of these experiments.

observation appears to contrast with recent reports of increasing basaltic glass dissolution rates with increasing aqueous sulphate concentrations at low pH (Flaathen et al., 2010), findings of higher forsterite dissolution rates in the presence of various organic ligands (Grandstaff, 1986; Wogelius and Walther, 1991; Hänchen et al., 2006; Morris and Wogelius, 2008; Olsen and Rimstidt, 2008; Krevor and Lackner, 2009), and publications of enhanced basalt dissolution rates in the presence of aqueous organic species (Eick et al., 1996; Oelkers and Gislason, 2001; Hausrath et al., 2009). However, fluid speciation calculations indicate that sulphate is a weak complexing ligand for aluminium and that in our reactive fluids the majority of Al is complexed by fluoride (cf. Table 3). As for the addition of DFOB, its concentration is only 10 μmolal but orders of magnitude higher than siderophore concentrations reported to be present in seawater (Vraspir and Butler, 2009). The addition of 10 μmolal DFOB is probably too low to cause a measurable effect on the dissolution rates, especially in the presence of fluoride. This assumption is substantiated by the fact that the afore-mentioned references on forsterite–organic ligand interaction found that the addition of mM range concentrations of dissolved organics was required to substantially increase dissolution rates. Furthermore, these studies concurred that the organic ligand effect was considerably reduced at low pH. Another factor is that DFOB may complex with the various aqueous cations in solution, including Mg^{2+}, limiting its sorption on mineral surfaces. The final steady-state during the SWC experimental series was obtained after adding 2 mmolal of carbonate ions to the reactive fluid. This addition of alkalinity increased the reactive fluid pH to 4.3. As a consequence of this pH rise, the rates of all three solids decreased. This rate decrease was expected as all the solids are comprised of phases whose dissolution rates decrease with increasing pH at acidic conditions (cf. Eqs. (2)–(5)). It seems unlikely that rates decreased due to an increase of dissolved inorganic carbon (DIC) concentration for two reasons. First, the addition of 2 mmolal DIC is small compared to the 114 mmolal DIC present in this fluid due to carbon dioxide dissolution in the 4 bar pCO_2 atmosphere of the experiment (modelled after Duan et al., 2006). Secondly, the effect of DIC on silicate mineral dissolution rates at *low* pH was previously investigated for plagioclase

Please cite this article in press as: Wolff-Boenisch D., et al. Dissolution of basalts and peridotite in seawater, in the presence of ligands, and CO_2: Implications for mineral sequestration of carbon dioxide. *Geochim. Cosmochim. Acta* (2011), doi:10.1016/j.gca.2011.07.004

Table 3
Logarithm of the activities of the major aqueous aluminium and sulphate species in the steady-state solutions from experimental series SWC for the basaltic glass, crystalline basalt, and peridotite.

Reference code	Aqueous species							
	Al_{tot}	Al^{3+}	AlF^{2+}	AlF_2^{+}	AlF_3	SO_4^{2-}	KSO_4^{-}	$AlSO_4^{+}$
Basaltic glass								
SWC-Cl	−5.24	−6.35	–	–	–	–	–	–
SWC-F	−4.57	−7.37	−5.50	−4.94	−5.97	–	–	–
SWC-SO_4	−4.53	−7.31	−5.47	−4.92	−5.98	−3.08	−4.41	−6.23
SWC-DFOB	−4.54	−7.34	−5.49	−4.93	−5.97	−2.97	−4.30	−6.14
SWC-CO_3	−5.46	−9.02	−6.73	−5.73	−6.34	−3.02	−4.35	−7.87
Crystalline basalt								
SWC-Cl	−5.67	−6.78	–	–	–	–	–	–
SWC-F	−5.61	−9.10	−6.84	−5.89	−6.53	–	–	–
SWC-SO_4	−5.79	−9.35	−7.06	−6.07	−6.68	−2.76	−4.10	−7.94
SWC-DFOB	−5.95	−9.49	−7.20	−6.22	−6.84	−3.48	−4.81	−8.80
SWC-CO_3	−6.02	−9.64	−7.32	−6.29	−6.87	−3.10	−4.43	−8.57
Peridotite								
SWC-Cl	−5.89	−7.00	–	–	–	–	–	–
SWC-F	−5.81	−9.32	−7.05	−6.08	−6.72	–	–	–
SWC-SO_4	−5.85	−9.38	−7.11	−6.13	−6.75	−3.63	−4.97	−8.85
SWC-DFOB	−6.06	−9.63	−7.33	−6.34	−6.95	−2.85	−4.18	−8.31
SWC-CO_3	−5.94	−9.56	−7.24	−6.22	−6.80	−3.18	−4.52	−8.57

(Carroll and Knauss, 2005), olivine (Hänchen et al., 2006; Prigiobbe et al., 2009a) and forsterite, diopside, wollastonite, and hornblende (Golubev et al., 2005). All these sources concluded that DIC only affects rates indirectly by changing pH as was observed in this experimental series.

Given that the difference between Si release rates from experiments performed under elevated CO_2 pressure and atmospheric conditions reported in the literature is relatively small, the following experimental series were performed at the same low pH by adding HCl to the inlet solution rather than applying elevated CO_2 pressure. By adding HCl we effectively titrate away the natural seawater alkalinity of the inlet fluids used during the F and DOC experimental series. This was done to deprive the system of its buffering capacity because the pCO_2 used during carbon storage efforts may be an order of magnitude higher than the 4 bar used during experimental series SWC.

Since the ionic strength of the SWC solutions corresponded to that of seawater, the next set of experiments was performed (a) to allow comparison with dissolution rates reported in the literature in a well established background electrolytes and (b) to investigate if specific seawater cations exert an influence on the dissolution rates of mafic and ultramafic rocks.

4.2. Experimental series I

Experimental series I was designed to illuminate the effect of ionic strength on silica release rates. Fig. 5 summarizes the results from this experimental series. Similar to experimental series SWC, basaltic glass and crystalline basalt exhibit comparable r_{Si}, while the peridotite releases Si four times faster at ionic strengths $\leqslant$31 mmol/kg (see Table 2). However, Si release rates from basalt increase with increasing ionic strength. As such, the difference between r_{Si} from basalt and peridotite decreases to less than a factor two at higher ionic strength.

The observation that r_{Si} from peridotite are independent of ionic strength and the identity of individual dissolved cations is in agreement with previous experimental results on olivine dissolution reported by Pokrovsky and Schott (2000) and Prigiobbe et al. (2009a). As the peridotite used in this study is olivine dominated, a direct comparison can be made between our results and forsterite dissolution rates reported in the literature. The geometric surface area normalized Si release rates from forsterite at pH ~3.6 range from $10^{-8.0}$ to $10^{-8.3}$ mol/m^2/s (Wogelius and Walther, 1991; Pokrovsky and Schott, 2000; Rosso and Rimstidt, 2000; Hänchen et al., 2006). These values are close to those of peridotite measured in this study, as listed in Table 2.

In contrast to peridotite, the Si release rates of basalt are influenced by the changing fluid composition in experimental series I. As both the identity of the dissolved cations changed and ionic strength was increased in the reactive fluids it is not possible to determine directly the cause for the changing basalt rates during this experimental series. Some literature evidence suggests this rate variation stems from the identity of the cation. Stockmann et al. (2011) studied the same glass as this study and observed that dissolution rates did not change when increasing reactive fluid ionic strength from 10 to 90 mmolal at pH 7 and 8. Silica polymorph dissolution rates, however, have been shown to depend on the identity of cations present in the reactive fluids including Mg, Ca, Na, and Pb. This phenomenon was accounted for by increased Si–O hydrolysis reactions in the solid-solution interface due to changing cation solvation properties (Dove and Crerar, 1990; Berger et al., 1994; Dove and Nix, 1997; Icenhower and Dove, 2000). Likewise, Kowacz and Putnis (2008) reported that mineral dissolution and precipitation rates can be modified by the

Please cite this article in press as: Wolff-Boenisch D., et al. Dissolution of basalts and peridotite in seawater, in the presence of ligands, and CO_2: Implications for mineral sequestration of carbon dioxide. *Geochim. Cosmochim. Acta* (2011), doi:10.1016/j.gca.2011.07.004

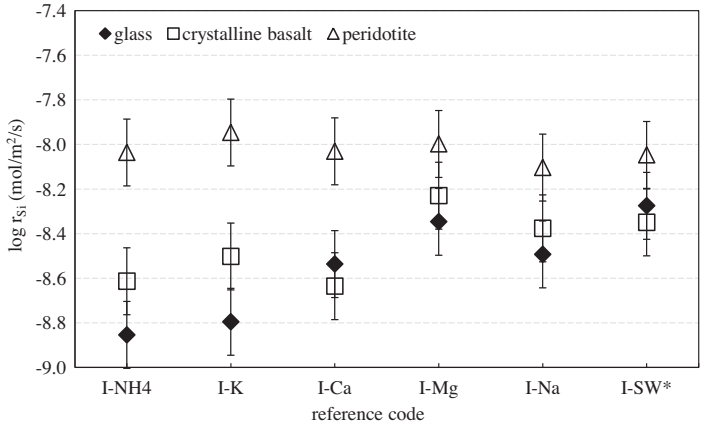

Fig. 5. Variation in steady-state Si release rates of the basaltic glass, crystalline basalt, and peridotite during experimental series I. The ionic strength increased from left to right.

introduction of simple ionic salts (KCl, NaCl, LiCl, CsCl, NaF, $NaNO_3$) to solution, based on the effects of these electrolytes on water structure dynamics and solute hydration. Tole et al. (1986) found that the addition of Na lowered nepheline dissolution rates. In contrast, other studies found no effect of the addition of cations to solution on rates. For example Rimstidt and Dove (1986) found no effect of Ca on wollastonite dissolution rates. Clearly, a more systematic approach is required to understand the effects of individual cations on mineral and rock dissolution rates.

A comparison of basalt dissolution rates is only meaningful if experiments were performed under similar experimental conditions, including ionic strength, and solution composition. Such comparisons can be made between the crystalline basalt rates measured in experiment I-NH_4 and rates reported by Gudbrandsson et al. (2011) which were performed on the same crystalline basalt as used in the present study. r_{Si} measured on crystalline basalt during experiment I-NH_4 at pH 3.6 is $10^{-8.6}$ mol/m^2/s. This values lies between r_{Si} values of $10^{-8.4}$ and $10^{-8.9}$ mol/m^2/s that Gudbrandsson et al. (2011) determined at pH 3 and 4, respectively. Correspondingly, basaltic glass dissolution rates measured during experiment I-NH_4 are $10^{-8.8}$ mol/m^2/s, consistent with a basaltic glass rate of $10^{-9.0}$ mol/m^2/s reported by Wolff-Boenisch et al. (2004b) at pH 4.

A comparison between peridotite Si release rates of experimental series I with those of the SWC series reveals that the presence of high CO_2 partial pressure increases rates by ~0.4 log units. Some previous work suggested an influence of CO_2 on such rates. For example, Golubev et al. (2005) found that forsterite dissolution rates are 0.2 log units higher in the presence of 1 bar pCO_2 compared to their CO_2-free experiments at pH 4.1. Forsterite dissolution rates reported by Hänchen et al. (2006) at 15–180 bar CO_2 pressure and pH 3–4 are consistently 0.3 log units higher than their CO_2-free counterparts. As for the basalts, a comparison of Si release rates from inlet solutions of similar ionic strength, pH, and chemical composition (SW-DFOB vs. I-SW*, cf. Table 2) shows that rates are 0.3 log units higher in the presence of CO_2. As crystalline basalt contains 16 vol% olivine, this observation is consistent with that of peridotite. No further attempt was made to interpret the effect of CO_2 on Si release as this effect is small, even at substantial CO_2 pressures.

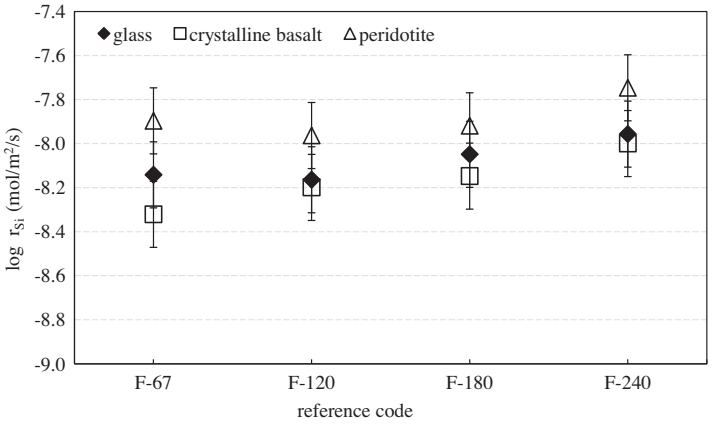

Fig. 6. Variation in steady-state Si release rates of the basaltic glass, crystalline basalt, and peridotite during experimental series F. The numbers after the dash is the targeted fluoride concentration in μmol/kg of the inlet fluid and increased from left to right (Table 2).

Please cite this article in press as: Wolff-Boenisch D., et al. Dissolution of basalts and peridotite in seawater, in the presence of ligands, and CO_2: Implications for mineral sequestration of carbon dioxide. *Geochim. Cosmochim. Acta* (2011), doi:10.1016/j.gca.2011.07.004

4.3. Experimental series F

The main purpose of experimental series F was to quantify the effect of increasing fluoride concentration on mafic and ultramafic rock dissolution. In this series, steady-state Si release rates were determined in acidified natural seawater to which NaF was sequentially added. In total, four steady-state rates were determined at distinct aqueous fluoride concentrations. The resulting r_{Si} are listed in Table 2 and plotted in Fig. 6. Like in the SWC series, the addition of aqueous fluoride minimally affects peridotite dissolution. In contrast, Si release rates from basalt increase with increasing aqueous fluoride concentration. The increase in Si release rates from basaltic glass, however, is less than what one might expect from the findings of Wolff-Boenisch et al. (2004a) who reported rate increases of up to an order of magnitude in the dissolution rates of various volcanic glasses at similar fluoride concentrations. To investigate these differences, r_{Si} of the crystalline (X) and glassy basalt (G) are compared to those of two basaltic reference glasses in Fig. 7. The chemical compositions of these glasses are listed in Table 1a. The crosses in this figure represent r_{Si} for the basaltic glass 'SS' and were published previously by Wolff-Boenisch et al. (2004a) whereas the open circles are release rates for basaltic glass 'HEI', which have not been previously published. These two basalt reference glasses were dissolved using similar mixed-flow reactor techniques and at comparable proton and fluoride concentrations, yet in a much weaker background electrolyte (10 mM NH_4Cl). Fig. 7 shows considerable overlap, not

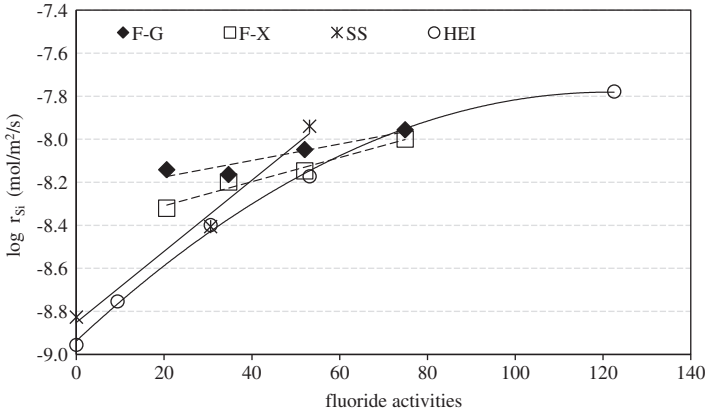

Fig. 7. Steady-state Si release rates of the basaltic glass (–G) and the crystalline basalt (–X) in the presence of varying fluoride activities during experimental series F. The initial inlet fluid for experimental series F was a natural seawater solution containing 67 μmolal fluoride, adjusted to pH 3.6 by adding HCl. After reaching steady-state, NaF was added to this inlet fluid to create inlet fluids containing fluoride concentrations of 120, 180, and 240 μmolal, respectively (Table 2). Also shown are rates and trend lines for the reference basaltic glasses SS (crosses) and HEI (open circles). Data for SS was retrieved from Wolff-Boenisch et al. (2004a,b). Note that the trend lines for SS and HEI (solid) are steeper than for G and X (dashed).

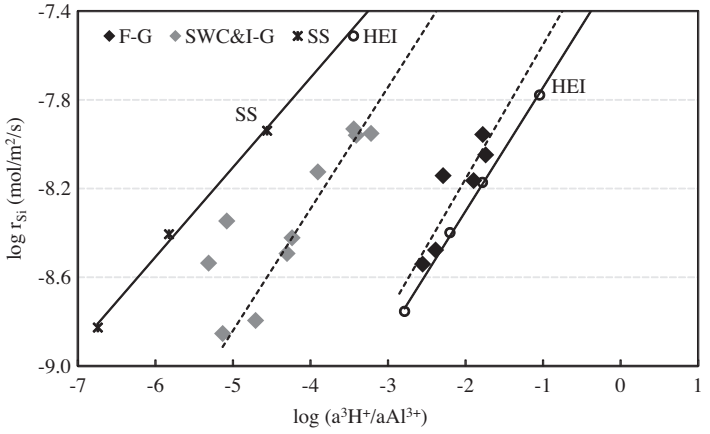

Fig. 8. Steady-state Si release rates of the basaltic glass (–G) as a function of the log $(a^3_{H^+}/a_{Al^{3+}})$. The black diamonds represent basaltic glass dissolution experiments from the F series and I-SW* carried out in natural seawater whereas the grey symbols stand for results of basaltic glass experiments from the SWC and I series (except for I-SW*). Also shown are rates and solid linear trend lines for the reference basaltic glasses SS (crosses) and HEI (open circles). Data for SS was retrieved from Wolff-Boenisch et al. (2004a,b). A linear relationship of rate versus aqueous activity ratio has been observed in the literature for volcanic glasses of varying composition and silica content and is consistent with Eq. (2).

Please cite this article in press as: Wolff-Boenisch D., et al. Dissolution of basalts and peridotite in seawater, in the presence of ligands, and CO_2: Implications for mineral sequestration of carbon dioxide. *Geochim. Cosmochim. Acta* (2011), doi:10.1016/j.gca.2011.07.004

only between individual basalt rates but also the projected crystalline (X) and glassy (G) rates at higher fluoride concentrations where the dashed lines meet the open circle. Only at very low fluoride activities do the glassy and

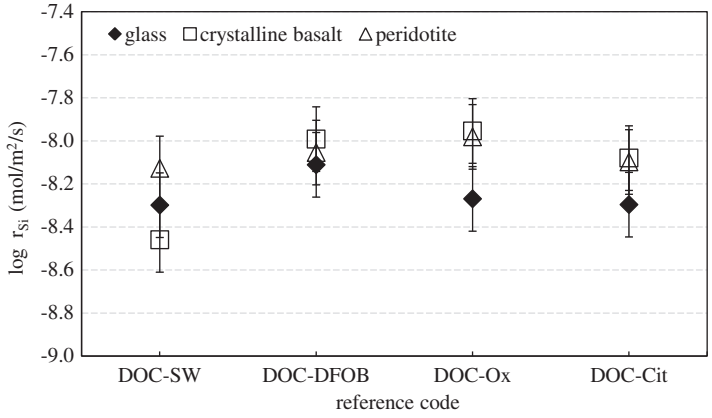

Fig. 9. Steady-state Si release rates of the basaltic glass, crystalline basalt, and peridotite during experimental series DOC. The initial inlet fluid for experimental series DOC was natural seawater adjusted to pH 3.6 with HCl. Subsequent reactive inlet fluids were composed of (1) this acidified seawater plus 120 μmolal DFOB, (2) this acidified seawater plus 120 μmolal oxalic acid, and (3) this acidified seawater plus 120 μmolal of citric acid (Table 2).

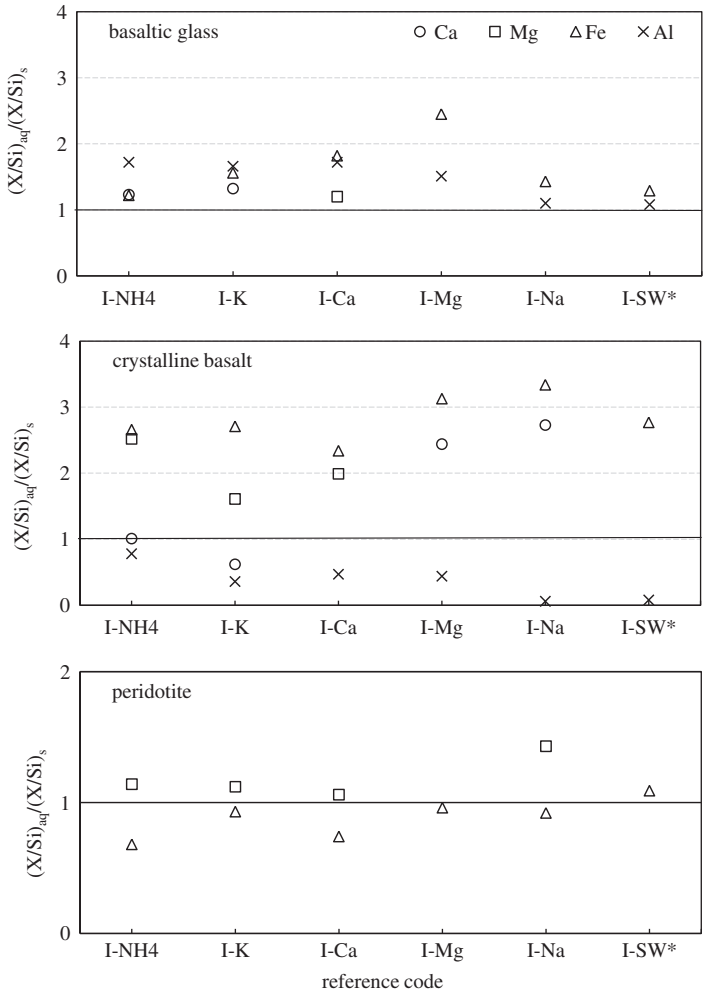

Fig. 10. Solute Si normalized elemental ratios (aq) divided by solid Si normalized elemental ratios (s) from the experimental series I where X = Ca, Mg, Fe, Al. A ratio of one corresponds to the stoichiometric dissolution of the rock and is shown as a black line in the figure.

Please cite this article in press as: Wolff-Boenisch D., et al. Dissolution of basalts and peridotite in seawater, in the presence of ligands, and CO_2: Implications for mineral sequestration of carbon dioxide. *Geochim. Cosmochim. Acta* (2011), doi:10.1016/j.gca.2011.07.004

crystalline basalts of this study exhibit considerably higher release rates than the basalt reference glasses causing the flatter slopes (dashed lines). As suggested by the results of experimental series I, these differences may stem from the influence of cation identity or ionic strength on rates.

To further illuminate the mechanism responsible for the increase of basaltic glass Si release rates with aqueous fluoride concentration these rates are plotted as a function of $a^3_{H^+}/a_{Al^{3+}}$ in Fig. 8. It can be seen in this figure that rates for each reference glass and for the glass G determined in experimental series SWC, I, and F plot as linear relationships consistent with Eq. (2). Note, however, that the different experimental series yield two distinct parallel linear trends. The presence of seawater tends to lower constant log $(a^3_{H^+}/a_{Al^{3+}})$ basaltic glass dissolution rates. The lower rates in the presence of seawater hint at a ligand saturation effect. Total ligand to aluminium concentration ratios (L_{tot}/Al_{tot}) of $\leqslant 3$ were found for the basaltic glass in experimental series SWC and I (except for I-SW*) whereas L_{tot}/Al_{tot} ratios of ≥ 7 were observed for the glass in experimental series F and I-SW* (the seawater experiments in Fig. 7). Thus, additional ligands in solution do not increase basalt rates proportionately to their overall concentration.

4.4. Experimental series DOC

The goal of the DOC experimental series was to estimate the effect of selected organic acids on Si release rates. Fig. 9 summarizes the results of this experimental series. The presence of 120 μmolal of DFOB, oxalate, or citrate affects only slightly basaltic glass and peridotite dissolution rates. Oelkers and Gislason (2001) found only a 0.2–0.3 log unit increase in basaltic glass dissolution rates by adding 1 mmolal oxalic acid, at pH 3. This finding agrees well with Eick et al. (1996) who found that the addition of 2 mM oxalic acid solution had only little effect on synthetic lunar basaltic glass dissolution rates at pH 3 and higher. The lack of an effect of the addition of organic ligands on basaltic glass dissolution rates in the present study may additionally be related to the use of seawater as a background fluid. As described above, in such fluids Al may be preferentially complexed with inorganic ligands such as fluoride rather than the added organic species. In contrast, r_{Si} from crystalline basalt increase 0.4–0.5 log units by the addition of 120 μmolal of DFOB, oxalate, or citrate to seawater. The source of the difference in dissolution behaviour exhibited by the basaltic glass and crystalline basalt observed in this study in response to the addition of organic ligands is probably related to the different mineralogy of these solids. Oelkers and Schott (1998) argued that aqueous Al complexation with organic ligands in solution explains the increase of alkali feldspars dissolution rates with increasing organic ligand concentration through Eq. (2). This process does not influence significantly the rates of Si release from crystalline basalts at acid pH, where such release rates are dominated by olivine and clinopyroxene dissolution (Gudbrandsson et al., 2011). In contrast, the observation that oxalate and citrate enhance the dissolution rates of olivine and clinopyroxene (Amrhein and Suarez, 1988; Shotyk and Nesbitt, 1990, 1992; Wogelius and Walther, 1991; Welch and Ullman, 1993, 1996; Stillings et al., 1996; Stephens and Hering, 2004; Golubev and Pokrovsky, 2006; Hänchen et al., 2006; Olsen and Rimstidt, 2008) has been attributed to a sorption mechanism (cf. Furrer and Stumm, 1986; Drever and Stillings, 1997; Ganor et al., 2009; Schott et al., 2009 and references cited therein). As r_{Si} of peridotite are unaffected by the addition of organic ligands to the fluid phase, it seems that the most likely source of organic ligand enhancement of Si release rates from crystalline basalt is the sorption of organic ligands to clinopyroxene.

5. CONCLUSIONS

This study explored the effects of different aqueous components on the dissolution of basalt and peridotite in acidified seawater. At 25 °C and pH 3.6, glassy and crystalline basalts exhibit similar silica release rates at varying ionic strengths and solution compositions, in accord with findings from Gudbrandsson et al. (2011). Only in the presence of specific ligands is there a clear distinction in dissolution kinetics between these basalts. For example, the glass is more sensitive to the presence of aqueous fluoride than the crystalline basalt. It is reasoned that the strong effect of aqueous fluoride on basaltic glass dissolution rates originates from the formation of aqueous aluminium–fluoride complexes in solution lowering the concentration of free aluminium in the reactive fluid. In contrast, Si release from crystalline basalt at low pH is dominated by olivine and clinopyroxene dissolution. The Si release rates of these minerals are less influenced by aqueous Al^{3+} activity explaining the contrasting behaviour of these two basalts. The effect of aqueous fluoride on basaltic glass dissolution in seawater is similar to previous glass dissolution studies performed in low ionic strength solutions. Only at low fluoride concentration is glass dissolution faster in seawater than in low ionic strength solutions. This observation may stem from the contribution of other ligands present in seawater for aqueous aluminium complexation.

Other ligands are found to have distinct effects on Si release rates. The presence of relatively low concentrations of organic acids only enhanced Si release rates from crystalline basalt. This increase may indicate surface complexation of the organic ligands on clinopyroxene surfaces. Surface complexation has been proposed to explain the dissolution promoting effect at low pH of oxalate and citrate on diopside (Golubev and Pokrovsky, 2006), thus it seems reasonable that such complexation also affects the dissolution rates of the augite present in crystalline basalts. r_{Si} of all solids are found to increase by 0.3–0.5 log units in the presence of a pCO_2 of 4 bar compared to atmospheric CO_2 pressure. This finding is consistent with previous studies and indicates a positive, yet unappreciated effect of CO_2 on silicate dissolution at low pH.

Perhaps the most significant observation of this study is the similarity of Si release rates of dunitic peridotite compared with that of basalt; r_{Si} from the dunitic peridotite are found to be not more than 0.6 log units faster than corresponding rates of crystalline basalt or basaltic glass at all conditions considered in this study. This observation

Please cite this article in press as: Wolff-Boenisch D., et al. Dissolution of basalts and peridotite in seawater, in the presence of ligands, and CO_2: Implications for mineral sequestration of carbon dioxide. *Geochim. Cosmochim. Acta* (2011), doi:10.1016/j.gca.2011.07.004

suggests that for the purposes of in-situ mineral sequestration, CO_2-charged seawater injected into basalt might be nearly as efficient a carbonatization process as injection into peridotite. Note that this conclusion probably also extends to peridotites found in ophiolite complexes, viz. lherzolite and harzburgite, as these peridotites also possess very low Al_2O_3 content.

6. IMPLICATIONS FOR MINERAL SEQUESTRATION OF CARBON DIOXIDE

In-situ carbonatization of CO_2 faces two major challenges, (a) the need to dissolve CO_2 to promote water/rock reactions and (b) permeability reductions in the host rock due to secondary mineral precipitation. Carbonates or any other secondary precipitate could reduce permeability to such an extent that injection will become impaired. Secondary mineral precipitation and solutions that become supersaturated with respect to one or more of the phases contained in the host rock may also slow the dissolution of primary minerals (Cubillas et al., 2005; Daval et al., 2011; Stockmann et al., 2011). A key to sustained carbon injection lies in sustaining the dissolution of reservoir rocks to preserve porosity and permeability. Reservoir rock dissolution is also crucial to obtain alkalinity, a prerequisite for carbonate precipitation (Wolff-Boenisch, 2011). In the light of the results presented above, the dissolution of CO_2 into seawater prior to or during its injection appears to be a promising approach. There is however a trade-off because saline solutions have lower CO_2 solubilities than low ionic strength solutions. Furthermore, it is essential to understand that the findings discussed above have been based on silica release rates while divalent metal release is essential for mineral sequestration. Unfortunately, many experiments in this study were carried out in artificial and natural seawater and therefore the information on these divalent cation release rates is irretrievable. However, the basaltic glass and peridotite can be viewed as homogeneous phases that dissolve congruently. This is corroborated in Fig. 10 that illustrates the solute X/Si ratios of elements released to the fluid divided by the solid X/Si ratios for the rocks from experimental series I. This series is the only one where additional concentrations for Ca and Mg besides Fe and Al could be determined. Congruent dissolution results in a stoichiometric ratio of one between solute and solid X/Si ratios. As can be seen in Fig. 10, the peridotite dissolves congruently and the vast majority of data points from the glassy basalt are consistent with its stoichiometric dissolution. The crystalline basalt releases divalent cations, especially Mg and Fe, two to three times faster than it releases Si. This is consistent with its dissolution being dominated by olivine and augite at low pH, as reported by Gudbrandsson et al. (2011). Taken together, the results shown in Fig. 10 suggest that to a first approximation, stoichiometric dissolution can be assumed for the glass and peridotite rates reported in this study. That means that per mole of rock (or Si) 0.75 and 1.76 moles of divalent cations are released from the basaltic glass and peridotite, respectively (cf. Table 1a). Divalent metal cations tend to be released approximately 2–3 times faster than Si from the crystalline basalt.

Some insight into potential mechanisms that would help increasing host-rock dissolution during mineral sequestration efforts can be attainted from this study. Results reported above show that filtered seawater of normal salinity increases r_{Si} of basalts compared to low ionic strength solutions to such an extent that they nearly match those of peridotite. Addition of aqueous fluoride to this fluid can increase the dissolution rates of glassy basalt yet further. The efficiency of relatively low equimolar concentrations of organic ligands in promoting mafic and ultramafic rock dissolution is minor for peridotite and basaltic glass but may be significant for crystalline basalt. Peridotite Si release rates only respond slightly to changes in seawater fluid chemistry. Basaltic glass dissolution is accelerated in the presence of fluoride whereas low concentrations of organic acids promote crystalline basalt Si release rates.

An added benefit of the addition to the fluid phase of ligands that can complex aqueous aluminium is that they could reduce the potential for the precipitation of secondary aluminosilicate phases that consume those divalent cations that could otherwise be used for carbonate precipitation. Seawater has the added advantage of high initial Ca and Mg concentrations such that the availability of divalent cations may not be the limiting or critical factor of carbonate precipitation but rather the aqueous carbonate concentration, which is governed by the pH and pCO_2. In contrast, the sulphate present in seawater may prove problematical as it is an inefficient Al-chelator and may interfere with the carbonatization process through anhydrite formation. Anhydrite solubility is retrograde and this mineral may, at least at higher temperatures, scavenge considerable amounts of Ca from solution and clog pore space. To avoid Ca-sulphates precipitation selective removal of sulphate from the injection fluid may be required. Sulphate extraction is carried out in oil production processes where seawater is routinely injected into oilfields to maintain pressure. The incompatibility of oil field formation waters and untreated seawater causes formidable sulphate scaling problems that are prevented by stripping the sulphate from the seawater (Bader, 2006, 2007).

In summary, the use of sulphate-free seawater with added fluoride to complex released aluminium seems to be a good starting point for a carbonation injection fluid. Note that natural seawater alkalinity caused the pH rise from 3.6 to 4.3 in experimental series SWC and might be considered an additional benefit of using seawater as carbonation solution. Nevertheless, at a modest injection pressure of $pCO_2 = 30$ - bar, the pH of equilibrated seawater is 3.6 (modelled using data retrieved from Duan et al. (2006) together with PHREEQC). Under these circumstances, the carbonic acid has titrated away all natural alkalinity.

As for the choice of host rock, peridotite releases more divalent cations per mole of rock when dissolved stoichiometrically compared to basaltic glass but this advantage is offset by the preferential release of divalent cations from crystalline basalt (see Gudbrandsson et al., 2011). Furthermore, the reactivities of glassy and crystalline basalt are more readily controlled by varying fluid chemistry.

Please cite this article in press as: Wolff-Boenisch D., et al. Dissolution of basalts and peridotite in seawater, in the presence of ligands, and CO_2: Implications for mineral sequestration of carbon dioxide. *Geochim. Cosmochim. Acta* (2011), doi:10.1016/j.gca.2011.07.004

Nevertheless, fluoride and/or organic additives to the injection fluid may increase the costs of carbon sequestration efforts. Further modelling and experimental work is required to refine these concepts and create an efficient carbonation fluid to maximize matrix dissolution and subsequent mineral trapping of carbon dioxide.

ACKNOWLEDGEMENTS

We thank our friends and colleagues Christian Grimm, Helgi Alfredsson, Eydis Eiriksdottir, Iwona Galeczka, Kiflom Mesfin, Snorri Gudbrandsson, and Gabrielle Stockmann. Holmfridur Sigurdardottir from Reykjavik Energy is gratefully acknowledged as well as Håkon Austrheim from the University of Oslo for generously providing the peridotite. This study was funded by 'The Environmental Fund of Reykjavik Energy' through the CarbFix project.

REFERENCES

Amrhein C. and Suarez D. L. (1988) The use of a surface complexation model to describe the kinetics of ligand-promoted dissolution of anorthite. *Geochim. Cosmochim. Acta* **52**, 2785–2793.

Andreani M., Luquot L., Gouze P., Godard M., Hoisé E. and Gibert B. (2009) Experimental study of carbon sequestration reactions controlled by the percolation of CO_2-rich brine through peridotites. *Environ. Sci. Technol.* **43**, 1226–1231.

Bader M. S. H. (2006) Sulfate scale problems in oil fields water injection operations. *Desalination* **201**, 100–105.

Bader M. S. H. (2007) Sulfate removal technologies for oil fields seawater injection operations. *J. Petrol. Sci. Eng.* **55**, 93–110.

Berger G., Cadore E., Schott J. and Dove P. M. (1994) Dissolution rate of quartz in lead and sodium electrolyte solutions between 25 and 300 °C: effect of the nature of surface complexes and reaction affinity. *Geochim. Cosmochim. Acta* **58**, 541–551.

Bischoff J. L. and Dickson F. W. (1975) Seawater–basalt interaction at 200 °C and 500 bars: implications for origin of sea-floor heavy-metal deposits and regulation of seawater chemistry. *Earth Planet. Sci. Lett.* **25**, 385–397.

Brandt F., Bosbach D., Krawczyk-Bärsch E., Arnold T. and Bernhard G. (2003) Chlorite dissolution in the acid pH-range: a combined microscopic and macroscopic approach. *Geochim. Cosmochim. Acta* **67**, 1451–1461.

Carroll S. A. and Knauss K. G. (2005) Dependence of labradorite dissolution kinetics on CO_2(aq), Al(aq), and temperature. *Chem. Geol.* **217**, 213–225.

Chen Y. and Brantley S. L. (2000) Dissolution of forsteritic olivine at 65 °C and $2 < pH < 5$. *Chem. Geol.* **165**, 267–281.

Cubillas P., Köhler S., Prieto M., Causserand C. and Oelkers E. H. (2005) How do mineral coatings affect dissolution rates? An experimental study of coupled $CaCO_3$ dissolution–$CdCO_3$ precipitation. *Geochim. Cosmochim. Acta* **69**, 5459–5476.

Daval D., Hellmann R., Corvisier J., Tisserand D., Martinez I. and Guyot F. (2010) Dissolution kinetics of diopside as a function of solution saturation state: macroscopic measurements and implications for modeling of geological storage of CO_2. *Geochim. Cosmochim. Acta* **74**, 2615–2633.

Daval D., Sissmann O., Menguy N., Saldi G. S., Guyot F., Martinez I., Corvisier J., Garcia B., Machouk I., Knauss K. and Hellmann R. (2011) Influence of amorphous silica layer formation on the dissolution rate of olivine at 90 °C and elevated pCO_2. *Chem. Geol.* **284**, 193–209.

de Leeuw N. H., Parker S. C., Catlow C. R. A. and Price G. D. (2000) Modelling the effect of water on the surface structure and stability of forsterite. *Phys. Chem. Mineral.* **27**, 332–341.

Devidal J.-L., Schott J. and Dandurand J.-L. (1997) An experimental study of kaolinite dissolution and precipitation kinetics as a function of chemical affinity and solution composition at 150 °C, 40 bars, and pH 2, 6.8, and 7.8. *Geochim. Cosmochim. Acta* **61**, 5165–5186.

Dixit S. and Carroll S. (2007) Effect of solution saturation state and temperature on diopside dissolution. *Geochem. Trans.* **8**, 3.

Dove P. M. and Crerar D. A. (1990) Kinetics of quartz dissolution in electrolyte solutions using a hydrothermal mixed flow reactor. *Geochim. Cosmochim. Acta* **54**, 955–969.

Dove P. M. and Nix C. J. (1997) The influence of the alkaline earth cations, magnesium, calcium, and barium on the dissolution kinetics of quartz. *Geochim. Cosmochim. Acta* **61**, 3329–3340.

Drever J. I. and Stillings L. L. (1997) The role of organic acids in mineral weathering. *Colloids Surf. A* **120**, 167–181.

Duan Z., Sun R., Zhu C. and Chou I. M. (2006) An improved model for the calculation of CO_2 solubility in aqueous solutions containing Na^+, K^+, Ca^{2+}, Mg^{2+}, Cl^-, and SO_4^{2-}. *Mar. Chem.* **98**, 131–139.

Eick M. J., Grossl P. R., Golden D. C., Sparks D. L. and Ming D. W. (1996) Dissolution kinetics of a lunar glass simulant at 25 °C: the effect of pH and organic acids. *Geochim. Cosmochim. Acta* **60**, 157–170.

Flaathen T. K., Gislason S. R. and Oelkers E. H. (2010) The effect of aqueous sulphate on basaltic glass dissolution rates. *Chem. Geol.* **277**, 345–354.

Furrer G. and Stumm W. (1986) The coordination chemistry of weathering: I. Dissolution kinetics of d-Al_2O_3 and BeO. *Geochim. Cosmochim. Acta* **50**, 1847–1860.

Ganor J., Reznik I. J. and Rosenberg Y. O. (2009) Organics in water–rock interactions. *Rev. Mineral. Geochem.* **70**, 259–369.

German C. R., Lin J., Parsons L. M. and Parson L. M. (2004) Mid-ocean ridges: hydrothermal interactions between the lithosphere and oceans. *Geophysical Monograph* **148**. American Geophysical Union, Washington, DC.

Gislason S. R. and Oelkers E. H. (2003) Mechanism, rates, and consequences of basaltic glass dissolution: II. An experimental study of the dissolution rates of basaltic glass as a function of pH and temperature. *Geochim. Cosmochim. Acta* **67**, 3817–3832.

Gislason S. R., Wolff-Boenisch D., Stefansson A., Oelkers E. H., Gunnlaugsson E., Sigurdardottir H., Sigfusson B., Broecker W. S., Matter J. M., Stute M., Axelsson G. and Fridriksson T. (2010) Mineral sequestration of carbon dioxide in basalt: a pre-injection overview of the CarbFix project. *Int. J. Greenhouse Gas Control* **4**, 537–545.

Golubev S. V., Pokrovsky O. S. and Schott J. (2005) Experimental determination of the effect of dissolved CO_2 on the dissolution kinetics of Mg and Ca silicates at 25 °C. *Chem. Geol.* **217**, 227–238.

Golubev S. V. and Pokrovsky O. S. (2006) Experimental study of the effect of organic ligands on diopside dissolution kinetics. *Chem. Geol.* **235**, 377–389.

Grandstaff D. (1986) The dissolution rate of forsteritic olivine from Hawaiian beach sand. In *Rates of Chemical Weathering of Rocks and Minerals* (eds. S. M. Colman and D. P. Dethier). Academic Press, Florida.

Greenough J. D. and Papezik V. S. (1985) Chloritization and carbonatization of Cambrian volcanic rocks in eastern Newfoundland and southern New Brunswick, Canada. *Chem. Geol.* **53**, 53–70.

Please cite this article in press as: Wolff-Boenisch D., et al. Dissolution of basalts and peridotite in seawater, in the presence of ligands, and CO_2: Implications for mineral sequestration of carbon dioxide. *Geochim. Cosmochim. Acta* (2011), doi:10.1016/j.gca.2011.07.004

Gudbrandsson S., Wolff-Boenisch D., Gislason S. R. and Oelkers E. H. (2011) An experimental study of crystalline basalt dissolution from $2 \leqslant pH \leqslant 11$ and temperatures from 5 to 75 °C. *Geochim. Cosmochim. Acta*, this issue, doi:10.1016/j.gca.2011.06.035.

Hänchen M., Prigiobbe V., Storti G., Seward T. M. and Mazzotti M. (2006) Dissolution kinetics of forsteritic olivine at 90–150 °C including effects of the presence of CO_2. *Geochim. Cosmochim. Acta* **70**, 4403–4416.

Harouiya N. and Oelkers E. H. (2004) An experimental study of the effect of aqueous fluoride on quartz and alkali-feldspar dissolution rates. *Chem. Geol.* **205**, 155–167.

Hausrath E. M., Neaman A. and Brantley S. L. (2009) Elemental release rates from dissolving basalt and granite with and without organic ligands. *Am. J. Sci.* **309**, 633–660.

Humphris S. E., Zierenberg R. A., Mullineaux L. S. and Thomson R. E. (1995) Seafloor hydrothermal systems: physical, chemical, biological, and geological interactions. *Geophysical Monograph* **91**. American Geophysical Union, Washington, DC.

Icenhower J. P. and Dove P. M. (2000) The dissolution kinetics of amorphous silica into sodium chloride solutions: effects of temperature and ionic strength. *Geochim. Cosmochim. Acta* **64**, 4193–4203.

Kelemen P. B. and Matter J. (2008) In situ carbonation of peridotite for CO_2 storage. *Proc. Natl. Acad. Sci. USA* **105**, 17295–17300.

Knauss K. G., Nguyen S. N. and Weed H. C. (1993) Diopside dissolution kinetics as a function of pH, CO_2, temperature, and time. *Geochim. Cosmochim. Acta* **57**, 285–294.

Kostenko O., Jamtveit B., Austrheim H., Pollok K. and Putnis C. (2002) The mechanism of fluid infiltration in peridotites at Almklovdalen, western Norway. *Geofluids* **2**, 203–215.

Kowacz M. and Putnis A. (2008) The effect of specific background electrolytes on water structure and solute hydration: consequences for crystal dissolution and growth. *Geochim. Cosmochim. Acta* **72**, 4476–4487.

Krevor S. C. and Lackner K. S. (2009) Enhancing process kinetics for mineral carbon sequestration. *Energy Procedia* **1**, 4867–4871.

Kuo L.-C. and Kirkpatrick R. J. (1985) Kinetics of crystal dissolution in the system diopside–forsterite–silica. *Am. J. Sci.* **285**, 51–90.

Lackner K. S., Wendt C. H., Butt D. P., Joyce E. L. and Sharp D. H. (1995) Carbon dioxide disposal in carbonate minerals. *Energy* **20**, 1153–1170.

Lackner K. S. (2003) Climate change: a guide to CO_2 sequestration. *Science* **300**, 1677–1678.

Lowell R. P., Seewald J., Metaxas A. and Perfit M. (2008) Magma to microbe: modeling hydrothermal processes at oceanic spreading centers. *Geophysical Monograph Series* **178**. American Geophysical Union, Washington, DC.

Lowson R. T., Comarmond M. C. J., Rajaratnam G. and Brown P. L. (2005) The kinetics of the dissolution of chlorite as a function of pH and at 25 °C. *Geochim. Cosmochim. Acta* **69**, 1687–1699.

Macrellis H. M., Trick C. G., Rue E. L., Smith G. and Bruland K. W. (2001) Collection and detection of natural iron-binding ligands from seawater. *Mar. Chem.* **76**, 175–187.

Marini L. (2006) The Kinetics of Mineral Carbonation. In *Developments in Geochemistry*, vol. 11. Elsevier (Chapter 6).

Matter J. M., Takahashi T. and Goldberg D. (2007) Experimental evaluation of in-situ CO_2–water–rock reactions during CO_2 injection in basaltic rocks: implications for geological CO_2 sequestration. *Geochem. Geophys. Geosyst.* **8**, Q02001.

McGrail B. P., Schaef H. T., Ho A. M., Chien Y.-J., Dooley J. J. and Davidson C. L. (2006) Potential for carbon dioxide sequestration in flood basalts. *J. Geophys. Res.* **111**, B12201.

Metz B., Davidson O., deConinck H., Loos M. and Meyer L. (2005) *IPCC Special Report on Carbon Dioxide Capture and Storage*. Cambridge University Press, New York.

Millero F. J. (2003) Physicochemical controls on seawater. In *The Oceans and Marine Geochemistry: Treatise on Geochemistry*, vol. 6 (eds. H. D. Holland and K. K. Turekian). Pergamon, Oxford.

Morris P. M. and Wogelius R. A. (2008) Phthalic acid complexation and the dissolution of forsteritic glass studied via in situ FTIR and X-ray scattering. *Geochim. Cosmochim. Acta* **72**, 1970–1985.

Mottl M. J. and Holland H. D. (1978) Chemical exchange during hydrothermal alteration of basalt by seawater: I. Experimental results for major and minor components of seawater. *Geochim. Cosmochim. Acta* **42**, 1103–1115.

Nakamura K. and Kato Y. (2004) Carbonatization of oceanic crust by the seafloor hydrothermal activity and its significance as a CO_2 sink in the Early Archean. *Geochim. Cosmochim. Acta* **68**, 4595–4618.

Oelkers E. H., Schott J. and Devidal J.-L. (1994) The effect of aluminum, pH, and chemical affinity on the rates of aluminosilicate dissolution reactions. *Geochim. Cosmochim. Acta* **58**, 2011–2024.

Oelkers E. H. and Schott J. (1998) Does organic acid adsorption affect alkali-feldspar dissolution rates? *Chem. Geol.* **151**, 235–245.

Oelkers E. H. and Schott J. (1999) Experimental study of kyanite dissolution rates as a function of chemical affinity and solution composition. *Geochim. Cosmochim. Acta* **63**, 785–797.

Oelkers E. H. (2001a) An experimental study of forsterite dissolution rates as a function of temperature and aqueous Mg and Si concentrations. *Chem. Geol.* **175**, 485–494.

Oelkers E. H. (2001b) General kinetic description of multioxide silicate mineral and glass dissolution. *Geochim. Cosmochim. Acta* **65**, 3703–3719.

Oelkers E. H. and Gislason S. R. (2001) The mechanism, rates and consequences of basaltic glass dissolution: I. An experimental study of the dissolution rates of basaltic glass as a function of aqueous Al, Si and oxalic acid concentration at 25 °C and $pH = 3$ and 11. *Geochim. Cosmochim. Acta* **65**, 3671–3681.

Oelkers E. H. and Schott J. (2001) An experimental study of enstatite dissolution rates as a function of pH, temperature, and aqueous Mg and Si concentration, and the mechanism of pyroxene/pyroxenoid dissolution. *Geochim. Cosmochim. Acta* **65**, 1219–1231.

Oelkers E. H. and Schott J. (2005) Geochemical aspects of CO_2 sequestration. *Chem. Geol.* **217**, 183–186.

Oelkers E. H., Gislason S. R. and Matter J. (2008a) Mineral carbonation of CO_2. *Elements* **4**, 333–337.

Oelkers E. H., Schott J., Gauthier J.-M. and Herrero-Roncal T. (2008b) An experimental study of the dissolution mechanism and rates of muscovite. *Geochim. Cosmochim. Acta* **72**, 4948–4961.

Oelkers E. H., Hering J. G. and Zhu C. (2011) Water: is there a global crisis? *Elements* **7**, 157–162.

Olsen A. A. and Rimstidt D. J. (2008) Oxalate-promoted forsterite dissolution at low pH. *Geochim. Cosmochim. Acta* **72**, 1758–1766.

Parkhurst D. L. and Appelo C. A. J. (1999) User's guide to PHREEQC (version 2) – a computer program for speciation, batch-reaction, one-dimensional transport, and inverse geochemical calculations. U.S.G.S. Wat. Res. Inv. Report.

Pokrovsky O. S. and Schott J. (2000) Kinetics and mechanism of forsterite dissolution at 25 °C and pH from 1 to 12. *Geochim. Cosmochim. Acta* **64**, 3313–3325.

Please cite this article in press as: Wolff-Boenisch D., et al. Dissolution of basalts and peridotite in seawater, in the presence of ligands, and CO_2: Implications for mineral sequestration of carbon dioxide. *Geochim. Cosmochim. Acta* (2011), doi:10.1016/j.gca.2011.07.004

Prigiobbe V., Costa G., Baciocchi R., Hänchen M. and Mazzotti M. (2009a) The effect of CO_2 and salinity on olivine dissolution kinetics at. *Chem. Eng. Sci.* **64**, 3510–3515.

Prigiobbe V., Hänchen M., Costa G., Baciocchi R. and Mazzotti M. (2009b) Analysis of the effect of temperature, pH, CO_2 pressure and salinity on the olivine dissolution kinetics. *Energy Procedia* **1**, 4881–4884.

Rimstidt J. D. and Dove P. M. (1986) Mineral/solution reaction rates in a mixed flow reactor: wollastonite hydrolysis. *Geochim. Cosmochim. Acta* **50**, 2509–2516.

Robins B. and Tysseland M. (1983) The geology, geochemistry and origin of ultrabasic fenites associated with the Pollen Carbonatite (Finnmark, Norway). *Chem. Geol.* **40**, 65–95.

Rogers K. L., Neuhoff P. S., Pedersen A. K. and Bird D. K. (2006) CO_2 metasomatism in a basalt-hosted petroleum reservoir, Nuussuaq, West Greenland. *Lithos* **92**, 55–82.

Rosso J. J. and Rimstidt J. D. (2000) A high resolution study of forsterite dissolution rates. *Geochim. Cosmochim. Acta* **64**, 797–811.

Schaef H. T. and McGrail B. P. (2009) Dissolution of Columbia River Basalt under mildly acidic conditions as a function of temperature: experimental results relevant to the geological sequestration of carbon dioxide. *Appl. Geochem.* **24**, 980–987.

Schaef H. T., McGrail B. P. and Owen A. T. (2010) Carbonate mineralization of volcanic province basalts. *Int. J. Greenhouse Gas Control* **4**, 249–261.

Schott J. and Oelkers E. H. (1995) Dissolution and crystallization rates of silicate minerals as a function of chemical affinity. *Pure Appl. Chem.* **67**, 903–910.

Schott J., Pokrovsky O. S. and Oelkers E. H. (2009) The link between mineral dissolution/precipitation kinetics and solution chemistry. *Rev. Mineral. Geochem.* **70**, 207–258.

Schwartz F. W. and Ibaraki M. (2011) Groundwater: a resource in decline. *Elements* **7**, 175–180.

Seifritz W. (1990) CO_2 disposal by means of silicates. *Nature* **345**, 486.

Seyfried W. E. and Bischoff J. L. (1977) Hydrothermal transport of heavy metals by seawater: the role of seawater/basalt ratio. *Earth Planet. Sci. Lett.* **34**, 71–77.

Seyfried W. E. and Bischoff J. L. (1979) Low temperature basalt alteration by sea water: an experimental study at 70 °C and 150 °C. *Geochim. Cosmochim. Acta* **43**, 1937–1947.

Seyfried W. E. and Bischoff J. L. (1981) Experimental seawater–basalt interaction at 300 °C, 500 bars, chemical exchange, secondary mineral formation and implications for the transport of heavy metals. *Geochim. Cosmochim. Acta* **45**, 135–147.

Seyfried W. E. and Mottl M. J. (1982) Hydrothermal alteration of basalt by seawater under seawater-dominated conditions. *Geochim. Cosmochim. Acta* **46**, 985–1002.

Shotyk W. and Nesbitt H. W. (1990) Ligand-promoted dissolution of plagioclase feldspar: a comparison of the surface chemistry of dissolving labradorite and bytownite using SIMS. *Chem. Geol.* **84**, 320–321.

Shotyk W. and Nesbitt H. W. (1992) Incongruent and congruent dissolution of plagioclase feldspar: effect of feldspar composition and ligand complexation. *Geoderma* **55**, 55–78.

Shikazono N., Harada H., Ikeda N. and Kashiwagi H. (2009) Dissolution of basaltic rocks and its application to underground sequestration of CO_2 – estimate of mineral trapping by dissolution–precipitation simulation. *Jpn. Mag. Mineral. Petrol. Sci.* **38**, 149–160.

Siegel D. I. and Pfannkuch H. O. (1984) Silicate mineral dissolution at pH 4 and near standard temperature and pressure. *Geochim. Cosmochim. Acta* **48**, 197–201.

Steel K. M., Besida J., O'Donnell T. A. and Wood D. G. (2001) Production of Ultra Clean Coal: Part I. Dissolution behaviour of mineral matter in black coal toward hydrochloric and hydrofluoric acids. *Fuel Process. Technol.* **70**, 171–192.

Stephens J. C. and Hering J. G. (2004) Factors affecting the dissolution kinetics of volcanic ash soils: dependencies on pH, CO_2, and oxalate. *Appl. Geochem.* **19**, 1217–1232.

Stillings L. L., Drever J. I., Brantley S. L., Sun Y. and Oxburgh R. (1996) Rates of feldspar dissolution at pH 3–7 with 0–8 mM oxalic acid. *Chem. Geol.* **132**, 79–89.

Stockmann G. J., Wolff-Boenisch D., Gislason S. R. and Oelkers E. H. (2011) Do carbonate precipitates affect dissolution kinetics? 1: Basaltic glass. *Chem. Geol.* **284**, 306–316.

Tole M. P., Lasaga A. C., Pantano C. and White W. B. (1986) The kinetics of dissolution of nepheline ($NaAlSiO_4$). *Geochim. Cosmochim. Acta* **50**, 379–392.

Veizer J., Hoefs J., Ridler R. H., Jensen L. S. and Lowe D. R. (1989) Geochemistry of Precambrian carbonates: I. Archean hydrothermal systems. *Geochim. Cosmochim. Acta* **53**, 845–857.

Vraspir J. M. and Butler A. (2009) Chemistry of marine ligands and siderophores. *Annu. Rev. Mar. Sci.* **1**, 43–63.

Welch S. A. and Ullman W. J. (1993) The effect of organic acids on plagioclase dissolution rates and stoichiometry. *Geochim. Cosmochim. Acta* **57**, 2725–2736.

Welch S. A. and Ullman W. J. (1996) Feldspar dissolution in acidic and organic solutions: compositional and pH dependence of dissolution rate. *Geochim. Cosmochim. Acta* **60**, 2939–2948.

Wogelius R. A. and Walther J. V. (1991) Olivine dissolution at 25 °C: effects of pH, CO_2, and organic acids. *Geochim. Cosmochim. Acta* **55**, 943–954.

Wogelius R. A. and Walther J. V. (1992) Olivine dissolution kinetics at near-surface conditions. *Chem. Geol.* **97**, 101–112.

Wolff-Boenisch D. (2004) Data on 17 Icelandic volcanic glasses and 1 Californian ignimbrite. Reports for the Science Institute, RH-03-2004, Science Institute, Reykjavik.

Wolff-Boenisch D. (2011) On the buffer capacity of CO_2-charged seawater used for carbonation and subsequent mineral sequestration. *Energy Procedia* **4**, 3738–3745.

Wolff-Boenisch D., Gislason S. R. and Oelkers E. H. (2004a) The effect of fluoride on the dissolution rates of natural glasses at pH 4 and 25 °C. *Geochim. Cosmochim. Acta* **68**, 4571–4582.

Wolff-Boenisch D., Gislason S. R., Oelkers E. H. and Putnis C. V. (2004b) The dissolution rates of natural glasses as a function of their composition at pH 4 and 10.6, and temperatures from 25 to 74 °C. *Geochim. Cosmochim. Acta* **68**, 4843–4858.

Wolff-Boenisch D., Gislason S. R. and Oelkers E. H. (2006) The effect of crystallinity on dissolution rates and CO_2 consumption capacity of silicates. *Geochim. Cosmochim. Acta* **70**, 858–870.

Yoshida T., Hayashi K.-i. and Ohmoto H. (2002) Dissolution of iron hydroxides by marine bacterial siderophore. *Chem. Geol.* **184**, 1–9.

Associate editor: Jeffrey C. Alt

Please cite this article in press as: Wolff-Boenisch D., et al. Dissolution of basalts and peridotite in seawater, in the presence of ligands, and CO_2: Implications for mineral sequestration of carbon dioxide. *Geochim. Cosmochim. Acta* (2011), doi:10.1016/j.gca.2011.07.004